

Conditional Generative Models for High-Resolution Range Profiles: Capturing Geometry-Driven Trends in a Large-Scale Maritime Dataset

Edwyn Brent*†

STIM, Mines Paris, PSL University
Fontainebleau, France
edwyn.brent@minesparis.psl.eu

Santiago Velasco-Forero*

STIM, Mines Paris, PSL University
Fontainebleau, France
santiago.velasco@minesparis.psl.eu

Rami Kassab†

ARC, Thales Land and Air Systems
Limours, France
rami.kassab@thalesgroup.com

Abstract—High-resolution range profiles (HRRPs) enable fast onboard processing for radar automatic target recognition, but their strong sensitivity to acquisition conditions limits robustness across operational scenarios. Conditional HRRP generation can mitigate this issue, yet prior studies are constrained by small, highly specific datasets. We study HRRP synthesis on a large-scale maritime database representative of coastal surveillance variability. Our analysis indicates that the fundamental scenario drivers are geometric: ship dimensions and the desired aspect angle. Conditioning on these variables, we train generative models and show that the synthesized signatures reproduce the expected line-of-sight geometric trend observed in real data. These results highlight the central role of acquisition geometry for robust HRRP generation.

Index Terms—HRRP, Generative Models, Geometry, Radar

I. INTRODUCTION

Over the past decades, advancements in radar technology have led to significant improvements in resolution. Consequently, targets are no longer depicted as single points, but can be shown as a two-dimensional grid. However, due to the high rotation rate of the radars and the vast surveillance area, processing all targets simultaneously is computationally demanding. To address this challenge, long-range radar systems often reduce the dimensionality of the detection grid for each target. The one-dimensional data obtained as a result of this process are called *High-Resolution Range Profiles* (HRRP).

In defense-related research, collecting large and diverse measured datasets is challenging. Unlike image classification, where abundant public data exist, radar datasets remain scarce. To address this, researchers often rely on simulations, though these typically require complex modeling or scaled targets [1]. Since HRRP data can be derived from more conventional radar echoes, simulating them is simpler than emulating the full acquisition process. The MSTAR dataset is frequently used for this purpose [2]–[5], but it includes only 500 samples across ten targets, limiting its utility for machine learning. As a result, most HRRP datasets involve only a few targets [3], [6], [7].

Submitted at Eusipco26. This work was performed using HPC resources from GENCI-IDRIS (Grant 2024-AD011014422R1).

One object can give rise to multiple HRRPs, depending on the acquisition scenario. Many targets, such as ships or aircraft, remain underrepresented in large-scale HRRP databases, both in quantity and diversity. Generative models can help fill these gaps by synthesizing missing objects and scenarios, with the ultimate goal of enriching datasets for recognition. However, large-scale studies on measured HRRP remain scarce, and foundational behaviors are not yet well documented. We therefore focus on characterizing global trends in a real, large-scale HRRP database, leaving task-specific recognition gains for future work. Our contributions can be summarized as follows:

- **Foundational set of conditions.** We identify a minimal yet effective set of conditions that guide ship HRRP generation: ship dimensions and the desired aspect angle. These parameters encapsulate key geometric properties, enabling the synthesis of coarse-scale structural features.
- **Geometry-driven insight at scale.** We recall a geometry-driven behavior in *surface-radar* HRRP data [8]. Using a *large-scale* dataset of ship measurements and metadata, we show that conditional generative models consistently capture and reproduce this geometric trend using our set of conditions.
- **Generalization across gaps.** Building on prior work [3], [9], our conditional models jointly address (i) *missing scenarios* for known ships and (ii) *unseen ships*, enabling credible HRRP generation across these gaps.

II. HIGH-RESOLUTION RANGE PROFILE BACKGROUND

A radar system receives echoes of its transmitted waveform, which, after undergoing standard processing steps [10], can be represented on a two-dimensional polar grid of amplitudes σ , referred to as the *radar cross section* (RCS). The amplitude is maximized when a target effectively reflects the incident signal back toward the radar. This echo is parameterized by two coordinates: the range r , corresponding to the distance from the radar, and the azimuth ϕ , corresponding to the angular position. A *range profile* is obtained by integrating σ tangentially over a detection cone spanning the angular interval $[\Phi, \Phi + \Delta\Phi]$. The spacing between consecutive range

bins r_i defines the radar range resolution, hereafter denoted by Δr . The polar grid comprises s cells in total, including those activated by the target. Although the azimuth ϕ also possesses a finite resolution, this component is absorbed into the amplitude of the curve after transformation into a high-resolution range profile. Formally, the HRRP at range bin r_i is given by $\text{HRRP}(r_i) = \sum_{\phi_j \in [\Phi, \Phi + \Delta\Phi]} \sigma(r_i, \phi_j)$.

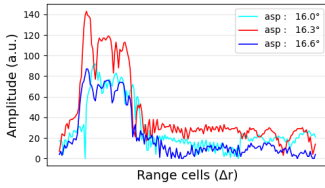


Fig. 1: Three different HRRP measurements of the same ship at nearby aspect angles.

the target heading (hdg) and the radar azimuth (ϕ), i.e., $\text{asp} = hdg - \phi$. The depression angle is the angle formed between the horizontal and the radar's *line of sight* (LOS). In [9], the authors show that a difference in aspect angle of one degree can produce significant differences in the acquired signal. Our data reproduce the same phenomenon (Fig. 1).

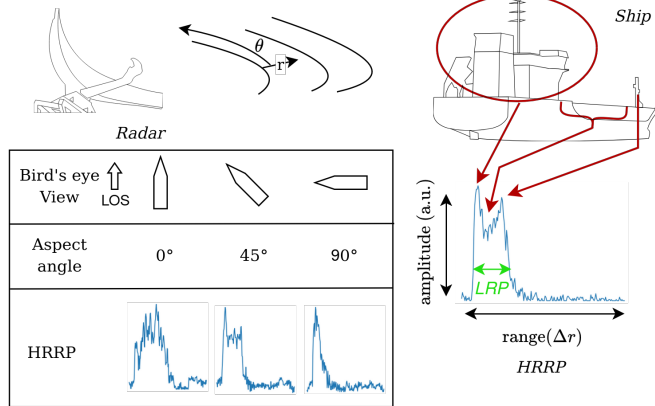


Fig. 2: Illustration of HRRP structure and its dependence on aspect angle: HRRP represents the amplitude of the combined echoes scattered by individual points within each range cell. Low-RCS parts of the ship cause drops in the HRRP, while high-RCS regions appear as peaks. The table highlights how aspect angle affects the coarse-scale structure of the HRRP by providing 3 data of the same ship at different aspect angles.

Numerous studies address HRRP-based target recognition, often using a single HRRP per target [11]–[13]. However, given the high variability of HRRP signals (Fig. 1) and their strong dependence on aspect angle (Fig. 2), these approaches are hard to scale to large datasets. An alternative is anomaly detection, which can focus on a specific target class and better generalize to unseen targets [14]. The impact of aspect angle is critical: in [5], the authors leverage contrastive learning with data augmentation to identify targets from HRRP captured at unseen views.

Classification performance ultimately depends on training data that reflect real-world diversity. Due to the limited size of radar datasets, synthetic HRRP generation is often used to fill in missing scenarios, most notably unseen aspect or depression angles [2], [4], [9]. However, these approaches remain limited, as they address angular gaps but overlook more critical issues such as label imbalance, which significantly impacts classification. A related effort in [3] tackles the missing-target problem, but its scope is hindered by a dataset of only three military vehicles, limiting both generalization and practical relevance.

III. PROPOSED METHOD

A. Overview

HRRP data are inherently challenging to interpret due to their sensitivity and the noise typically present in radar measurements. These data correspond to projections of radar echoes onto the radar's LOS. A fundamental property that arises from this formulation is the variation of the ship's apparent length in the HRRP as a function of its aspect angle [8]. This relationship can be expressed as

$$TLOP(L, W, \text{asp}) = L|\cos(\text{asp})| + W|\sin(\text{asp})| \quad (1)$$

where Theoretical Length of Object Projection (TLOP) denotes the projection of the vessel on the radar's LOS, while L and W correspond to the ship's length and width, respectively. The parameter asp represents the vessel's aspect angle at the time of HRRP acquisition. To recall the empirical TLOP in HRRP data as defined in [8], we first identify cells representing the ship's echo by smoothing the signal with a uniform filter, thresholding at 50% of the maximum amplitude, and closing gaps shorter than 14 cells to keep the object contiguous. This yields the empirical Length on Range Profile (LRP) as the span between the first and last selected bins. The threshold and gap size are chosen to balance noise rejection. We empirically verified that this process yields a robust LRP estimate. The strong correlation between LRP and TLOP (Fig. 5) demonstrates the validity of this approach.

As a first step toward faithful HRRP synthesis, we aim to match the TLOP distribution observed in real data; reproducing this coarse geometric statistic is a prerequisite for any further realism.

B. Conditioning Generative Models for HRRP

We compare two generative paradigms: Denoising Diffusion Probabilistic Models (DDPM) [15] and Generative Adversarial Networks (GAN) [16] for HRRP synthesis. Our objective departs from conventional unconditional generation: rather than maximizing generic sample diversity, we seek controllable generation tied to target attributes. To this end, we condition the model on ship length, width, and aspect angle (collectively represented by the vector c), which enforces the global structure of the generated HRRP. In both architectures, conditioning is applied by adding learned embeddings between every downsampling and upsampling stage.

1) *Denoising Diffusion Probabilistic Models (DDPMs):* Building on the classifier-free conditioning approach [17], our training process employs the following loss function

$$\mathcal{L}_{cddpm} = \mathbb{E}_{t, x_0, \epsilon, c} \left[\left\| \epsilon - \epsilon_\theta (\sqrt{\bar{\alpha}_t} x_0 + \sqrt{1 - \bar{\alpha}_t} \epsilon, t, c) \right\|^2 \right] \quad (2)$$

2) *Conditioning GANs:* We use a Wasserstein GAN (WGAN) [18] as a second generative model architecture. In the following equations, q denotes the data distribution and p the latent distribution. We train the WGAN by computing alternatively the generator loss,

$$\mathcal{L}_{advG} = - \mathbb{E}_{z \sim p, c} [D(G(z, c))] \quad (3)$$

and the discriminator loss

$$\mathcal{L}_{advD} = \mathbb{E}_{z \sim p, x \sim q, c} [D(G(z, c)) - D(x)]. \quad (4)$$

We use a Wasserstein GAN loss formulation. We enforce the critic's 1-Lipschitz constraint using weight clipping by clamping each parameter to the range $[-0.05, 0.05]$ after every discriminator update. Also, we augment the adversarial objective with a mean-squared-error (MSE) reconstruction term to promote signal-level fidelity between the real data x and the generated samples $G(z, c)$. The MSE loss is defined as

$$\mathcal{L}_{mse} = \mathbb{E}_{z \sim p, x \sim q, c} \left[\|x - G(z, c)\|^2 \right]. \quad (5)$$

To balance the contributions of each loss term, we introduce a weighting factor λ . Since the data are normalized, MSE loss is typically smaller in magnitude compared to the adversarial loss. Therefore, we set $\lambda = 50$ in all experiments. The discriminator is trained with \mathcal{L}_{advD} , while the generator minimizes

$$\mathcal{L}_{totG} = \mathcal{L}_{advG} + \lambda \mathcal{L}_{mse}. \quad (6)$$

IV. EXPERIMENTAL SETUP AND FINDINGS

A. Dataset

We leverage a large database of ship HRRP data acquired by a coastal radar system over several months. This dataset contains over 900k HRRP samples from more than 700 unique ships, covering a wide range of acquisition scenarios typical of coastal surveillance. Each HRRP is associated with metadata including the ship's Maritime Mobile Service Identity (MMSI), dimensions (length and width) and the aspect angle at acquisition, defined as the angle between the ship's heading and the radar's line of sight.

We collect our raw data using a ground-based radar located slightly above sea level. Given its elevation (around 100m) and the typically much larger range to targets, we consider the impact of the depression angle on HRRP data to be negligible. We therefore focus on the effect of the aspect angle, as it significantly influences the radar cross-section and the resulting HRRP.

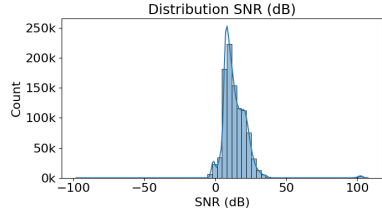


Fig. 3: Dataset SNR distribution.

Using the LRP calculation from Sec. (III-A), we estimate for each HRRP data the noise part and the signal part of the data. We then compute the SNR as the ratio between the average power of the signal part and the average power of the noise part. Figure 3 shows the SNR distribution in our dataset. We observe that most data have an SNR between 10dB and 30dB, with an average of 13dB, indicating a reasonable signal quality for our generative tasks.

We use the MMSI (a unique identifier for each ship) to select specific ships for the test dataset to ensure no overlap with the training data. In all experiments, the training dataset represents 90% of the entire dataset, and the validation and test datasets represent half of the remaining 10% of MMSI (still containing 100k data). We randomly select MMSI to fill the test/validation datasets and select the same way half of this set to fill in the validation dataset and the other half for the test dataset. Figure 4 shows the distribution of ship lengths and widths in the train and val/test datasets.

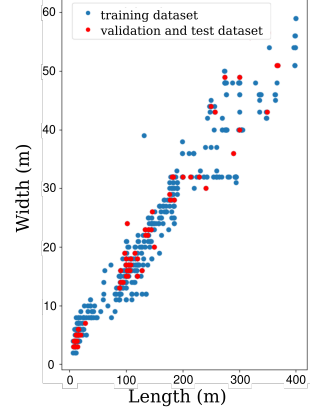


Fig. 4: Dataset ship dimensions. **Blue:** train, **Red:** val/test.

We adopt lightweight architectures to limit overfitting on low-dimensional HRRP data. The proposed GAN has 697k parameters (including 146k for the discriminator), and the DDPM has 730k. Both models are built upon 1D convolutional ResBlocks [19]. Aspect angles are encoded with sinusoidal embeddings, concatenated with the length and width, mapped through linear layers, and injected into the network by addition to the feature maps between successive downsampling and upsampling stages. We use a cosine noise schedule with 800 diffusion timesteps throughout training, which helps balance sample quality and computational efficiency.

B. Evaluation Metrics

Previous works on HRRP generation [2], [3], [9] primarily assess the benefit of generated data through classification accuracy improvements. In contrast, our goal conditions do not carry class information, classification would therefore not be meaningful. Thus, we evaluate generation fidelity using the metrics from [8], also enabling cross-paper comparison.

Due to the high sensitivity of HRRP to aspect angle (Fig. 1), pointwise comparisons with a single reference are unreliable. Instead, for each test sample, we define a local set of real

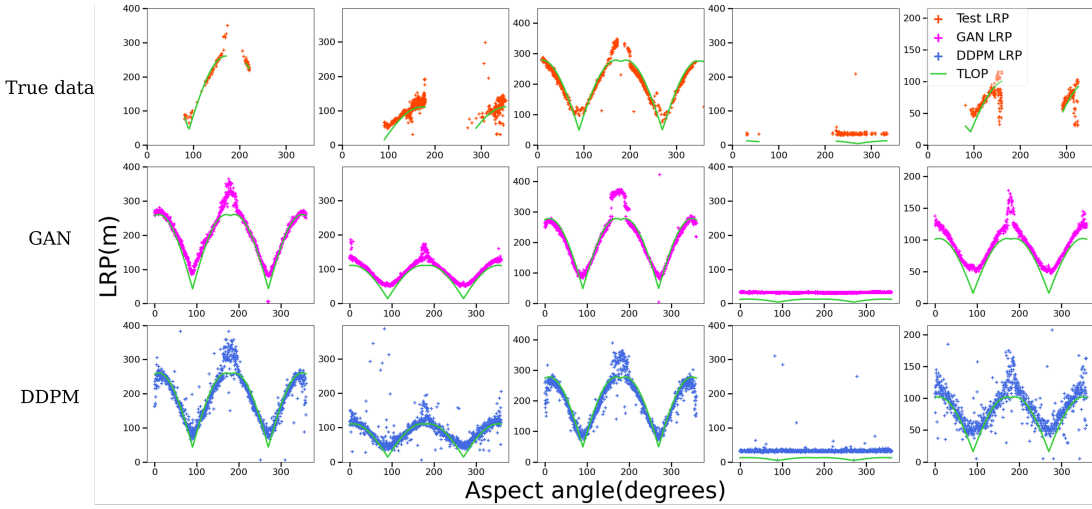


Fig. 5: LRP profiles from test data and samples generated with the proposed models. **Top:** test LRPs; gaps in aspect angles reflect missing measurements. **Middle:** GAN-generated LRPs conditioned on aspect angle, which follow the main trend but do not reproduce outliers. **Bottom:** LRPs measured on DDPM-generated HRRP conditioned on aspect angle, capturing both the trend and the outliers. **Green:** theoretical ship projection (TLOP, Eq. (1)). The different columns correspond to different ships of various dimensions. Overall, LRPs from generated and test data follow the TLOP trend.

HRRP within a small angular window $[\text{asp} - \Delta, \text{asp} + \Delta]$, compute metrics between each generated data and all elements in this set, retain the best match, and average these best scores over the test set. A generation is considered successful if it closely matches any real trace in its neighborhood. In practice, we set $\Delta = 2^\circ$ to define a narrow neighborhood. We generate a single sample per condition and select the closest real HRRP within a $\pm 2^\circ$ neighborhood; thus, the “best match” is taken over real neighbors, and full distribution matching is left for future work.

We adopt the MSE_f and \cos_f metrics from [8], and additionally compute PSNR restricted to activated cells in order to align with other metrics. The \cos_f metric quantifies the fidelity of scatter patterns within the signal, while MSE_f and PSNR provide global measures of similarity between the generated data and the ground-truth neighborhood. As the MSE_f is the most general metric, we use it to define the closest match in the neighborhood for PSNR and \cos_f calculations.

C. Results

As shown in Fig. 5, for both architectures, the *LRP* correlates strongly with the theoretical projection (*TLOP*). GAN-generated profiles follow the *TLOP* trend across aspect angles but miss the dataset outliers. DDPM-generated HRRP display a realistic trade-off: they capture both the outliers and the main trend. The test data departs from the *TLOP* for aspect angles of 180° , likely due to the influence of the bridge of the ship, not accounted for in the simple projection model. This effect is well captured by the generative models. For very small ships, the *TLOP* model is less accurate, certainly due to the relatively large resolution of the radar system compared to the ship size. This effect is also well captured by the generative models. Table I presents the generation metrics

TABLE I: Generation metrics for different models and conditioning types. The best scores for each model are in **bold**.

Model	Conditioning	PSNR \uparrow	$\text{MSE}_f \downarrow$	$\cos_f \uparrow$
GAN	none	15.7	11.6	0.33
	aspect angle	17.4	9.2	0.42
	dimensions	23.5	3.2	0.66
	aspect & dimensions	27.0	0.95	0.87
DDPM	none	15.8	13.0	0.38
	aspect angle	16.3	12.5	0.43
	dimensions	22.0	4.31	0.62
	aspect & dimensions	24.7	1.51	0.81

obtained in our experiments. We observe that conditioning with the dimensions, providing a strong prior on the HRRP structure, has the most significant impact on generation quality. However, adding aspect angle conditioning further improves performance, demonstrating that both conditions are complementary. Both models show similar trends, demonstrating this behavior is not method-dependent. Overall, the GAN achieves higher scores, likely due to the smoothing effect of the MSE loss, as discussed below.

We provide a comparative figure of the generated data and measured data (Fig. 6). The GAN model with full conditioning provides a similar match to the DDPM, but its signal is smoother. This phenomenon is likely due to the MSE loss used in the GAN training, which encourages averaging over possible outputs. On the contrary, the DDPM model generates signals with more variability, closer to real data but the smoothing phenomenon helps the GAN achieving higher metrics scores. Overall, both models using all conditions generate HRRP data with similar structures to real data of the same ship yet missing some fine details because of the coarse conditioning.

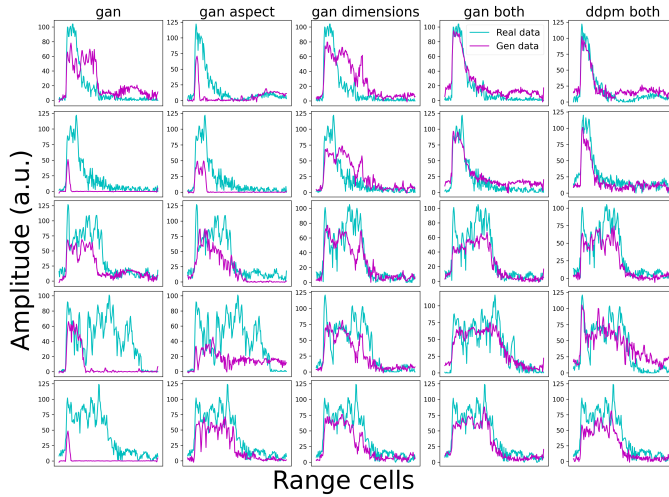


Fig. 6: Comparative figure of the generated HRRP (cyan) and the closest RP data of the same ship in the dataset within the 2° aspect angle tolerance (magenta). The columns correspond to different models and conditioning, and the rows to different ships. We observe that before conditioning with both the aspect angle and dimensions, the overlap between generated and real data is lower than using both.

D. Discussion

We do not target ship identification in this work. The models are conditioned only on coarse geometry (length, width, aspect angle) and deliberately avoid identity cues, so naive data augmentation for classification could introduce label noise. Our aim here is to characterize and reproduce global, geometry-driven structure in HRRP at scale, providing a foundation for future recognition-aware extensions using richer conditioning.

This study highlights that, despite the sensitivity of HRRP data to acquisition conditions, consistent patterns can still be learned and exploited in large-scale HRRP datasets. Our generative models leverage shared features among ships with similar dimensions, but incorporating richer conditioning could further improve fidelity. To support future work, we release a subset of modified data and generated samples for reproducibility, available at: <https://github.com/EdwynBrient/HRRPGen-geometry>.

V. CONCLUSION

We present the first study on HRRP generation using a large-scale dataset capturing the diversity of coastal radar surveillance scenarios. Our analysis highlights the mutual dependence between the conditioning variables, namely the target dimensions and aspect angle. The generated signatures reproduce the TLOP geometric property observed in real HRRP data. Finally, our conditional models achieve promising performance while relying on conditions that do not uniquely characterize the target, underscoring the fundamental role of these variables in HRRP synthesis.

REFERENCES

- [1] Jiacheng Bao et al., “Fine-grained image generation network with radar range profiles using cross-modal visual supervision,” *IEEE Transactions on Microwave Theory and Techniques*, vol. 72, no. 2, pp. 1339–1352, 2024.
- [2] Qiang Zhou, Yanhua Wang, Xin Zhang, Liang Zhang, and Teng Long, “Domain-adaptive hrrp generation using two-stage denoising diffusion probability model,” *IEEE Geoscience and Remote Sensing Letters*, vol. 21, pp. 1–5, 2024.
- [3] Liangchao Shi et al., “One-shot HRRP generation for radar target recognition,” *IEEE Geoscience and Remote Sensing Letters*, vol. 19, pp. 1–5, 2022.
- [4] Yue Huang et al., “Recognition-aware hrrp generation with generative adversarial network,” *IEEE Geoscience and Remote Sensing Letters*, vol. 19, pp. 1–5, 2022.
- [5] Yijin Zhong et al., “Contrastive learning for radar HRRP recognition with missing aspects,” *IEEE Geoscience and Remote Sensing Letters*, vol. 20, pp. 1–5, 2023.
- [6] Jinwei Wan et al., “Convolutional neural networks for radar hrrp target recognition and rejection,” *EURASIP J. Adv. Signal Process.*, vol. 2019, pp. 5, 2019.
- [7] Osman Karabayir et al., “Synthetic-range-profile-based training library construction for ship target recognition purposes of scanning radar systems,” *IEEE Transactions on Aerospace and Electronic Systems*, vol. 56, no. 4, pp. 3231–3245, 2020.
- [8] Edwyn Brient, Santiago Velasco-Forero, and Rami Kassab, “Mfn decomposition and related metrics for high-resolution range profiles generative models,” in *RadarConf25*, 2025.
- [9] Yiheng Song et al., “Multi-view hrrp generation with aspect-directed attention gan,” *IEEE Journal of Selected Topics in Applied Earth Observations and Remote Sensing*, vol. 15, pp. 7643–7656, 2022.
- [10] M.A. Richards, *Fundamentals Of Radar Signal Processing*, McGraw-Hill Education (India) Pvt Limited, 2005.
- [11] Chih-Lung Lin et al., “Radar high-resolution range profile ship recognition using two-channel convolutional neural networks concatenated with bidirectional long short-term memory,” *Remote Sensing*, vol. 13, no. 7, 2021.
- [12] Yujia Diao et al., “CNN based on multiscale window self-attention mechanism for radar HRRP target recognition,” in *2022 7th International Conference on Signal and Image Processing (ICSIP)*, 2022, pp. 281–285.
- [13] Bin Xu, Bo Chen, Jinwei Wan, Hongwei Liu, and Lin Jin, “Target-aware recurrent attentional network for radar HRRP target recognition,” *Signal Processing*, vol. 155, pp. 268–280, 2019.
- [14] Martin Bauw et al., “From unsupervised to semi-supervised anomaly detection methods for HRRP targets,” in *RadarConf20*. IEEE, 2020, pp. 1–6.
- [15] Jonathan Ho, Ajay Jain, and Pieter Abbeel, “Denoising diffusion probabilistic models,” in *Advances in Neural Information Processing Systems (NeurIPS)*, H. Larochelle, M. Ranzato, R. Hadsell, M.F. Balcan, and H. Lin, Eds. 2020, vol. 33, pp. 6840–6851, Curran Associates, Inc.
- [16] Ian J. Goodfellow, Jean Pouget-Abadie, Mehdi Mirza, Bing Xu, David Warde-Farley, Sherjil Ozair, Aaron Courville, and Yoshua Bengio, “Generative adversarial nets,” in *Advances in Neural Information Processing Systems*, Z. Ghahramani, M. Welling, C. Cortes, N. Lawrence, and K.Q. Weinberger, Eds. 2014, vol. 27, Curran Associates, Inc.
- [17] Jonathan Ho and Tim Salimans, “Classifier-free diffusion guidance,” in *NeurIPS 2021 Workshop on Deep Generative Models and Downstream Applications*, 2021.
- [18] Martin Arjovsky, Soumith Chintala, and Léon Bottou, “Wasserstein generative adversarial networks,” in *ICML*. PMLR, 2017, pp. 214–223.
- [19] Kaiming He, Xiangyu Zhang, Shaoqing Ren, and Jian Sun, “Deep residual learning for image recognition,” in *2016 IEEE Conference on Computer Vision and Pattern Recognition (CVPR)*, 2016, pp. 770–778.